Performance optimization and kinetic analysis of HNO₃ coupled with microwave rapidly modified coconut shell activated carbon for VOCs adsorption

Xing Rong[1,2†], Qing Cao[2†], Yan Gao[2,3]*, Xin Du[4], Huawei Dou[2,3], Min Yan[2], Shijie Li[2], Qian Wang[2], Zhanchao Zhang[3] and Baoming Chen[2]

[1]Shandong High Speed Maintenance Group Co. Ltd., Jinan, China, [2]Shandong Technology Innovation Center of Carbon Neutrality, School of Thermal Engineering, Shandong Jianzhu University, Jinan, China, [3]Shandong Province Jinan Ecological and Environmental Monitoring Center, Jinan, China, [4]Shandong Luqiao Group Equipment Technology Development Company, Jinan, China

As a typical carbon-based material, activated carbon (AC) has satisfied adsorption performance and is of great significance in the field of volatile organic compounds (VOCs) pollutants removal. In order to further reveal the optimization mechanism of AC adsorption performance, coconut shell-based AC was selected as the research object, and different concentrations of HNO₃ coupled with microwave were used for rapid modification and activation. The characteristic changes of pore structure and surface chemical of AC before and after rapid modification were analyzed, and the performance changes of VOCs absorption were discussed from the perspective of reaction kinetics. The pore structure and surface chemical properties of before and after modification were analyzed by X-ray diffraction (XRD), Scanning Electron Microscopy (SEM), Brunauer-Emmeta-Teller (BET) analysis, Fourier Transform Infrared Spectroscopy (FTIR), and Boehm titration. The results showed that HNO₃ coupled with microwave could significantly eliminate impurities in the pores of AC. After impregnation in HNO₃ at a concentration of 1.5 mol L⁻¹ and under microwave irradiation of 900 W, the number of micropore on the surface of samples increased slightly. When the impregnation concentration of HNO₃ continued to increase, the two adjacent pore structures of the samples merged, which lead to a large decrease in the number of micropore and a corresponding increase in the proportion of mesoporous. Meanwhile, the specific surface area S_{BET} of the modified NAC-6 sample increased to 1,140.40 m² g⁻¹, and the total acidic oxygen-containing functional groups on the surface increased by 0.459 mmol g⁻¹ compared to that of the unmodified raw carbon. Furthermore, by analyzing the experimental results of formaldehyde adsorption on AC samples, it was concluded that the saturated adsorption capacity of the modified NAC-6 sample was 43% higher than that of the raw carbon. This study provides a more convenient and faster modification method for AC in the field of gas phase pollutants purification, which is helpful to realize

the practical engineering application of AC with high efficiency, energy saving and sustainable.

1 Introduction

Volatile organic compounds (VOCs) are precursors of PM2.5 and ozone. By controlling VOCs, the synergistic control of PM2.5 and ozone can be strengthened, which is of great significance to realize the synergistic effect of pollution reduction and carbon reduction and promote the continuous improvement of ecological environment quality (Du et al., 2018; Gao et al., 2022). Formaldehyde is one of the most representative toxic VOCs in indoor pollutants, which can cause great harm to human health. When people inhale high concentrations of formaldehyde, it will cause irritation to mucosa and skin (Awadallah and Al-Muhtaseb, 2019; Gao et al., 2021). If people are exposed to low-dose formaldehyde for a long time, it can cause chronic poisoning, which will weaken the respiratory function of the body, disorder the information integration function of the nervous system and affect the immune response of the body (Shao et al., 2019; Civioc et al., 2020). The World Health Organization's International Agency for Research on Cancer (IARC) added formaldehyde to its latest list of carcinogens (Zhu et al., 2021). Therefore, exploring the effective way to remove indoor formaldehyde is one of the current research hotspots (Zahed et al., 2022).

In recent decades, various effective formaldehyde purification technologies have been explored, including adsorption, membrane separation, catalytic combustion and photocatalytic degradation (Gao et al., 2018; Chang et al., 2020; Ryu et al., 2022). Among them, the adsorption method has been considered as one of the most practical and effective technologies because of its low cost, simple operation and good treatment effect (Gao et al., 2019; Yu et al., 2019). Activated carbon (AC) is widely used as an adsorbent for the removal of pollutants due to its large specific surface area and abundant surface functional groups (Isinkaralar et al., 2022). It has obvious advantages in the treatment of gaseous pollutants, such as benzene, toluene, formaldehyde, etc (Saqlain et al., 2021). However, the extensive use of traditional activated carbon raw materials, such as coal and wood, will cause large consumption of fossil fuels and huge losses of forest resources, and significantly reduce the environmental friendliness of AC. Meanwhile, the AC derived from biomass waste is becoming a research hotspot of new carbon materials due to its wide source, low cost and environmental friendliness. However, the performance of biomass derived AC still needs to be optimized (Inal et al., 2020).

Regulating the functional groups and internal structure of carbon-based materials is a key factor to improve their adsorption performance (Demiral et al., 2021). The adsorption of VOCs by AC mainly depends on the physical adsorption of gas molecules by micropore in its structure, but the adsorption capacity is limited. Therefore, by means of modifying and improving the functional group status on the surface of AC, the adsorption of VOCs by AC can be transformed from physical adsorption to physical-chemical combined adsorption, so as to improve the adsorption performance of AC on VOCs(Du et al., 2018).

In order to satisfy the selective adsorption function for various pollutants, AC is required to have the appropriate proportion of mesopore and micropore (Hu et al., 2022). Meanwhile, the purpose of pore adjustment is to make the AC pore size close to the molecular size of pollutants, so as to achieve selective adsorption. Furthermore, the purpose of structural modification is to obtain AC with larger specific surface area in order to exhibit higher adsorption performance. The pore structure and surface chemical properties of AC can be changed by microwave heating (Zhang et al., 2023).

The adsorption performance of AC prepared from olivine by microwave modification was better than that of the raw AC. Compared with the unmodified AC, the specific surface area of the modified AC was increased by 27.48%, and the adsorption capacity of Fe^{2+} was 62.50 mg/g (Alslaibi et al., 2014). The adsorption capacity of modified AC on methylene blue (MB) and remazole brilliant violet dyes was studied by microwave treatment. Compared with the raw carbon, the modified AC had higher adsorption capacity and faster adsorption rate for MB and dye, because the AC micropores were expanded and more active adsorption sites were obtained (Khasri and Ahmad, 2018). Surface modification of activated carbon was carried out by microwave as heat source. The results showed that the carbon treated by microwave would be oxidized more or less, and most of the oxygen-containing groups were removed from the surface. Even under these conditions, it still had better surface properties than the raw carbon (Li et al., 2016). The effect of modified AC on the adsorption performance of SO_2 was studied by microwave heating technology (Zhang et al., 2016). The AC with various particle sizes was modified under different microwave power and irradiation time. The results showed that after microwave treatment of AC, the surface acidic oxygen-containing functional groups were reduced, and the basic characteristics were enhanced, which was also the main reason for the increase of the adsorption performance of activated carbon to SO_2 (Qu et al., 2021).

The surface functional groups of AC can be modified by various methods, including acid/alkali treatment, chemical oxidation or impregnation of metal elements (Abdulrasheed et al., 2018). The acid-base properties of AC surface have a significant effect on the adsorption performance. In the study of AC adsorption of phenol, when the basic groups on the surface of AC increase greatly, the phenolic hydroxyl groups on the aromatic ring were close to the carbonyl groups on the surface of AC, and the adjacent orbitals overlapped to form new bonds, thus improving the adsorption performance of AC for phenol (Li et al., 2020). The carbonyl group on the surface of AC could also provide electrons to the benzene ring in phenol to form electron pairs, thereby strengthening the adsorption of phenol by AC (Rungrodnimitchai and Hiranphinyophat, 2020).

HNO_3 modification increased the acid groups on the surface of AC, which could improve the adsorption of gaseous pollutants. From the perspective of surface chemical properties and structural characteristics, the modification of AC by HNO_3 significantly increased the acidic groups on the AC surface, especially the carboxyl groups (Liang et al., 2020). At the same time, the content of basic groups on the surface was seriously reduced and almost disappeared. It was found that the adsorption performance of acetanilide on AC modified by HNO_3 and H_2SO_4 was enhanced. As exhibited in the experiment of AC modified by HNO_3 and $(NH_4)_2S_2O_8$, the low concentration of HNO_3 treatment improved the microporous structure of AC samples, while high concentration of HNO_3 destroyed the porous structure (Toledo et al., 2020).

The oxygen-containing functional groups on the surface of AC are related to its preparation method, oxidation conditions and porous properties of AC. Compared with physical oxidation treatment, the surface of AC after HNO_3 oxidation treatment has both abundant oxygen-containing functional groups and higher acidity. However, the modification of coconut shell AC by HNO_3 oxidation can lead to the reduction of pore structure. After HNO_3 modification, although the acid oxygen-containing groups on the surface of AC samples increased, the BET specific surface area and the total pore volume of the modified AC showed a decreasing trend compared with the original carbon (Rungrodnimitchai and Hiranphinyophat, 2020). But the adsorption capacity of the modified AC for formaldehyde was higher than that of the unmodified activated carbon. It can be seen that acid modification changes the surface acidity and oxygen-containing functional group content of AC, thereby improving the selectivity and adsorption capacity of gaseous pollutants (Tan et al., 2019).

By analyzing the concentration breakthrough curve and temperature breakthrough curve of adsorbed pollutants, it is found that the adsorption process is dominated by the diffusion effect of micropores. The effects of pore structure and surface chemical properties of AC on the adsorption of benzene (gas) were studied. It was found that the larger the proportion of pore size <0.7 nm, the better the adsorption effect of AC on benzene,

and when there were oxygen-containing groups on the surface of AC, the adsorption performance would be better (Zhang et al., 2020; Yang et al., 2022). The presence of hydroxyl groups can increase the adsorption capacity of AC for VOCs. When AC adsorbs acetone, the smaller the pore size of AC, the stronger the effective diffusion of micropore depended on. After acid solution impregnation modification, the polarity of AC sample was enhanced, and the surface acidic groups were increased, so that the adsorption effect of AC on polar adsorbates became stronger.

According to the above research, it could be recognized that the modification of AC by microwave had the function of pore-forming and pore-expanding. The micropore structure of AC was enriched by microwave irradiation. However, microwave also affected the AC chemical properties at a certain extent. Compared with the raw carbon, the content of acid oxygen-containing functional groups on the surface of the regenerated AC was relatively reduced under the microwave radiation. At the same time, the basic functional groups were increased, resulting in the polarity reduction of the regenerated AC, which was not conducive to the adsorption of polar substances by AC. And the AC modified by acid can increase the content of oxygen-containing functional groups on the surface, improve the internal pore structure, and enhance the adsorption capacity of the sample to polar substances. This technology is suitable for the purification of polar gas phase pollutants. In this study, coconut shell-based AC was selected as the main research object, and different concentrations of HNO_3 coupled with microwave irradiation were used to modify AC by rapid impregnation. The pore structure and surface functional groups of AC samples before and after modification were determined by XRD, SEM, BET, FTIR and Boehm titration. Using formaldehyde, a typical indoor gas pollutant, as a probe molecule, the adsorption properties of the AC samples were evaluated by dynamic and static adsorption experiments, and the modification mechanism and reaction kinetics of the rapid treatment of biochar by HNO_3 coupled with microwave were studied. This paper will enrich the theoretical research of AC in the removal of air pollutants and propose an efficient AC modification method.

2 Materials and methods

2.1 Materials preparations

The raw AC was coconut shell derived carbon with specific surface area of $924.1 \, m^2 \, g^{-1}$, 80–120 mesh, particle size 0.12–0.18 mm (Jianxin activated carbon factory, Tangshan, China). At first, the raw AC was repeatedly cleaned with deionized water to remove surface dust and impurities. After drying at 110°C for 36 h, the pre-treated activated carbon was placed in a desiccator for use. Four parts of 10 g pretreated

activated carbon were put into a 300 ml conical flask, and then added to HNO_3 solution (AR, 68 wt%, laiyang Kant chemical, China) with molar concentrations of $2\,mol\,L^{-1}$, $4\,mol\,L^{-1}$, $6\,mol\,L^{-1}$ and $8\,mol\,L^{-1}$, respectively, soaked under the microwave irradiation of 900 W at 70°C for 4 h. The filtered samples were placed in a blast drying oven and dried at 110°C for 36 h for later use. The final sample was denoted as NAC-x (x = 2,4,6,8), x was the impregnation concentration of HNO_3 solution. Moreover, the unmodified AC was named NAC-0.

2.2 Materials characterizations

The crystal phase structure of the samples was determined by X-ray diffraction analysis (XRD), recorded on a Bruker D8 Advance powder diffractometer with reference to the International Center for Diffraction Data (ICDD). The surface morphology of AC before and after modification was observed by scanning electron microscope (SEM) on a Zeiss MERLIN Compact ultra-high resolution field emission scanning electron microscope. The surface area and pore size distribution of the samples were measured by N_2 adsorption-desorption isotherms at −196°C using specific surface area analyzer *via* an American Macdonald Station Extended Specific Surface and Porosity Analyzer ASAP 2460. A Germany Brooke Infrared Spectrometer TENSOR-27 was used to test Fourier Transform Infrared (FTIR) Spectrometer to compare the changes of oxygen-containing functional groups on the surface of AC before and after modification. The spectral resolution was $4\,cm^{-1}$, the scanning wavelength range was $4,000–500\,cm^{-1}$, and the scanning times were 16. Boehm titration quantitative analysis was used to further determine the specific differences in oxygen-containing functional groups of the samples. The static adsorption value of formaldehyde gas on modified AC samples under different concentration of HNO_3 was measured by phenol reagent-visible spectrophotometry.

2.3 Adsorption experiments

Static adsorption experiment was to investigate the formaldehyde saturation adsorption capacity of AC before and after modification in the atmosphere saturated with formaldehyde. At room temperature, a gas generation device was used to introduce the formaldehyde gas through the quartz tube equipped with AC sample. Meanwhile, the two ends of the quartz tube were blocked with quartz cotton, and the bubble tube equipped with formaldehyde absorption solution was used to absorb the exhaust gas. Before the adsorption experiment, the impurities affecting the experimental results in the quartz tube were purged out by background gas of N_2. The residual concentration of formaldehyde was measured by phenol reagent-visible spectrophotometry. After 24 h of continuous adsorption, the absorbance of the remaining absorption liquid in the colorimetric tube was evaluated and measured at 630 nm of the spectrophotometer. At this time, the evaluation of adsorption effect was determined by the amount of formaldehyde removed by the sample at adsorption equilibrium.

The formaldehyde dynamic adsorption experiment focused on the real-time dynamic adsorption of formaldehyde on AC. In this experiment, the real-time dynamic adsorption curve was drawn according to the adsorption amount of formaldehyde in AC samples at different times. Finally, the saturation time was obtained when the sample adsorption reached dynamic equilibrium. A 300 mg sample was weighed and placed in a quartz tube, both ends of which were blocked with quartz cotton. Similarly, before the adsorption experiment, the sample was first removed from the impurity in N_2 flow. The formaldehyde gas flowed through the sample at a rate of 80 ml/min, and the exhaust from the reaction tube was directed to a gas chromatograph (GC), where the concentration was recorded every 10 min.

2.3 Theoretical analysis model

In the study of adsorption system, the adsorption isotherm must be considered, because it showed the distribution of adsorbate between gas phase and solid phase at different equilibrium concentrations.

The Langmuir equation assumes that multilayer adsorption occurred on solid surface with active sites, while the adsorbent molecules occupy only a single point for the adsorption of monolayer molecules, which formed the adsorption-desorption dynamic model. However, multilayer adsorption was still the main method in practice. The Freundlich model is based on the assumption that multilayer adsorption occurred on heterogeneous surfaces and was applicable to a larger range.

The model is described in detail as following:

Langmuir formula of isothermal absorption (Giraldo et al., 2020; Prokic et al., 2020)

$$q_e = \frac{\alpha q_m c_e}{1 + \alpha c_e} \qquad (1)$$

Freundlich formula of isotherm adsorption (Vikrant et al., 2019a; Zhang et al., 2019)

$$q_e = k_f \left(c_e\right)^n \qquad (2)$$

Where q_e $(mg \cdot g^{-1})$ was the calculated adsorption capacity, c_e $(mg \cdot m^{-3})$ was the equilibrium concentration, α $(m^3 \cdot mg^{-1})$ was Langmuir adsorption model constant, q_m $(mg \cdot m^{-3})$ was saturated adsorption capacity of monolayer adsorption, k_f was Freundlich adsorption model constant, n was Freundlich adsorption model index.

In order to further understand the adsorption mechanism of formaldehyde on modified samples, quasi-first-order and quasi-second-order fitting adsorption kinetics models were used to fit and analyze the experimental data. The hypothesis of quasi-first-order fitting adsorption kinetic equation assumed that the adsorption process was physical adsorption, and the number of AC adsorption sites determined the adsorption rate of the

FIGURE 1
XRD patterns of the as-prepared AC samples.
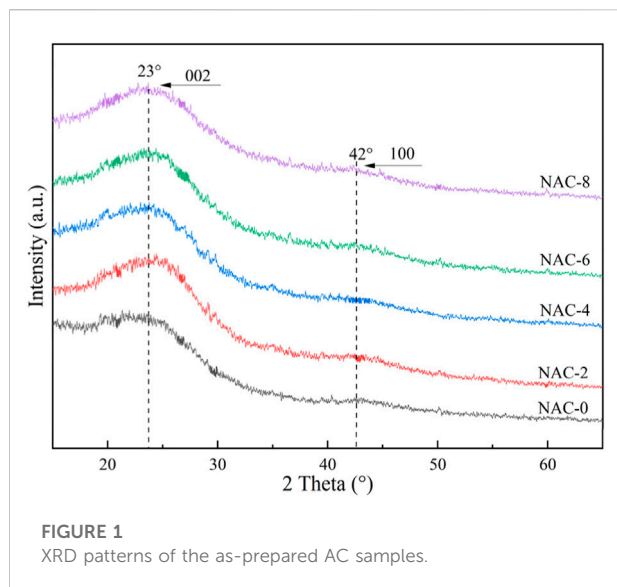
adsorbent. The quasi-second-order fitting of the adsorption kinetic equation assumed that the adsorption process was a combination of physical and chemical adsorption.

The quasi-first-order fitted adsorption kinetic equation (Vikrant et al., 2019b)

$$log\left(Q_e - Q_t\right) = logQ_e - \frac{k_1}{2.303}t \tag{3}$$

The quasi-second-order fitted adsorption kinetic equation (Cai et al., 2016)

$$\frac{t}{Q_t} = \frac{1}{k_2Q_e^2} + \frac{1}{Q_e}t \tag{4}$$

Where Q_e (mg·g^{-1}) and Q_t (mg·g^{-1}) were the equilibrium adsorption capacity at saturation and the instantaneous adsorption capacity at t-time, respectively. k_1 (min^{-1}) was a quasi-first-order adsorption constant, k_2 (g·mg^{-1}·min^{-1}) was the quasi-second-order adsorption constant. All kinetic models and isotherm models were fitted to experimental data using nonlinear equations. Non-linear regression analysis was performed, since the non-linear modeling was considered the best for estimating kinetic and isotherm parameters, due to the inherent bias, diverse estimation errors, and fit distortions, which might be resulting from the linearization.

3 Results and discussion

3.1 Structural characterization

3.1.1 XRD analysis

The crystallinity of NAC-x was analyzed by XRD as shown in Figure 1. The as-prepared AC showed broad peaks, indicating the amorphous structure. The broad peak in the range of 20–30° could be assigned to the (002) plane of amorphous carbon (Ryu et al., 2022). And the broad hump in the range of 40–50° was related to the (100) plane, which was caused by diffusion scattering of the amorphous carbon (Giraldo et al., 2020). After the AC was modified with HNO$_3$, the (002) plane peak of the sample NAC-x was significantly enhanced compared with the (100) plane peak of the unmodified raw carbon NAC-0, indicating that the pore structure in the modified AC was clearer and more developed.

3.1.2 Microscopic morphology analysis

Figure 2 showed the SEM scanning images of the AC samples before and after modification with a magnification of 3,000 times. According to Figure 2A, it was found that the surface of unmodified NAC-0 was rough and had many honeycomb pores, in which there were a large number of fine carbon particles or inorganic components. The surface pore structure of NAC-2 modified by HNO$_3$ with a concentration of 2 mol L^{-1}, as shown in Figure 2B, was evenly distributed, and the carbon particles were partially removed, but the pore structure did not change significantly. With the increase of HNO$_3$ concentration, the impregnation of HNO$_3$ at a concentration of 4 mol L^{-1} had a more obvious elimination effect on the fine particles in the internal structure of NAC-4 as shown in Figure 2C. When the concentration of HNO$_3$ was 6 mol L^{-1}, the internal pore structure of the modified NAC-6 was clearer and more orderly, the pore wall became thinner, the surface pores developed more open, and the pore structure converted clearer, but a small amount of pore structure was destroyed, as shown in Figure 2D. When the concentration of HNO$_3$ rose to 8 mol L^{-1}, the carbon structure lamellar of NAC-8 was eroded due to the high concentration of acid, and the pore wall was also seriously damaged. In some areas, adjacent pores merged to form super-large pores, as shown in Figure 2E. Therefore, the excessive oxidation caused by high concentration of HNO$_3$ could lead to the corrosion and structural collapse of AC pores.

3.1.3 BET pore structure analysis

Figure 3 showed the N$_2$ adsorption-desorption isothermal curve before and after AC modification. The structural characteristic parameters of the samples were shown in Table 1. According to the IUPAC classification method of N$_2$ adsorption, when the relative pressure $P/P_0 < 0.1$, the N$_2$ adsorption of the raw NAC-0 and the modified NAC-x with different concentrations of HNO$_3$ all conformed to the type I micropore adsorption. The N$_2$ adsorption capacity increased sharply and tended to be saturated with the increase of relative pressure P/P_0, indicating that there were a large number of micropore in AC before and after modification. In addition, it could be seen from Figure 3A that the shape of adsorption isotherms before and after modification had basically not changed. When the concentration of HNO$_3$ was 2 mol L^{-1},
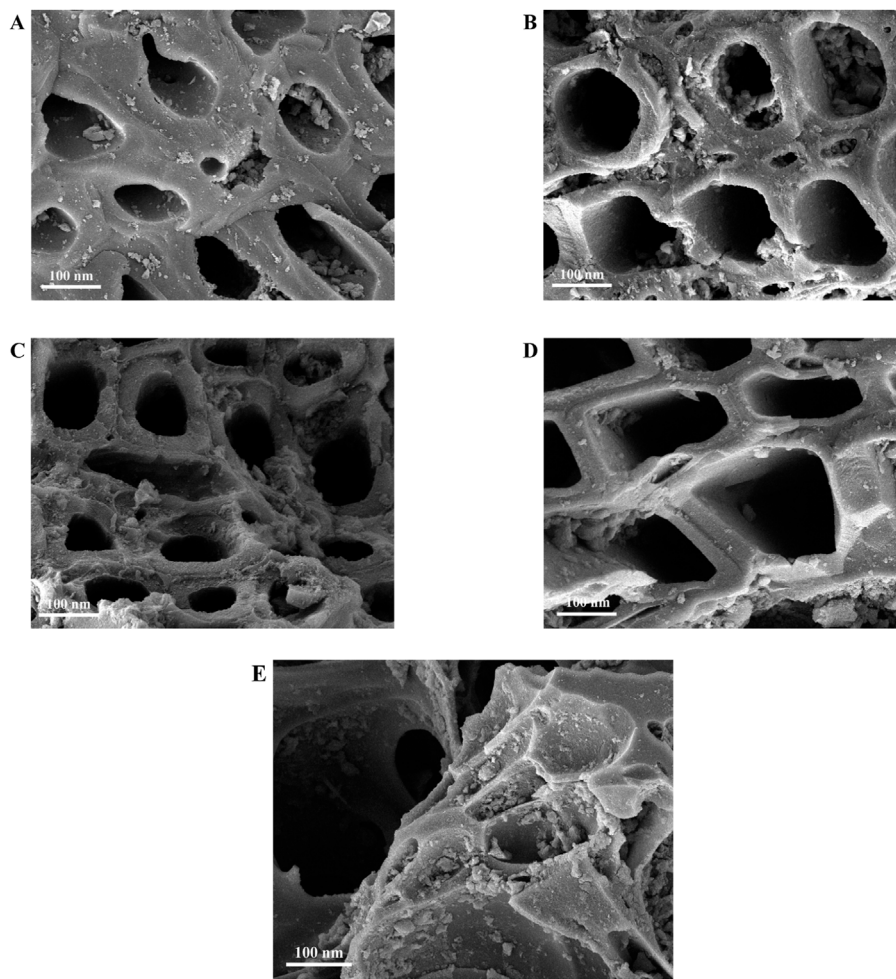
FIGURE 2
SEM images of as-prepared activated carbon samples: **(A)** NAC-0; **(B)** NAC-2; **(C)** NAC-4; **(D)** NAC-6; **(E)** NAC-8.
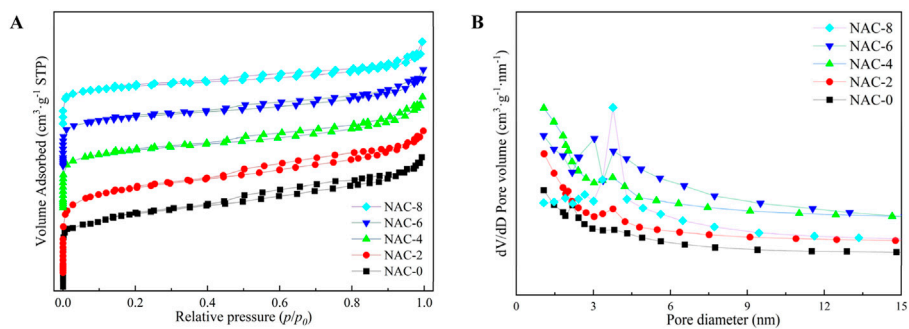
FIGURE 3
Pore structure analysis: **(A)** N_2 sorption isotherms; **(B)** pore-size distributions of the as-prepared AC samples.

TABLE 1 BET surface areas and pore size distributions of the as-prepared AC samples.

Samples	S_{BET} (m²·g⁻¹)	S_{mic} (m²·g⁻¹)	P_{mic} (%)	P_{mes} (%)	D (nm)
NAC-0	905.72	636.63	70.29	29.71	2.8
NAC-2	949.62	721.05	75.93	24.07	3.0
NAC-4	983.51	724.45	73.66	26.34	3.0
NAC-6	1140.40	804.21	70.52	29.48	3.2
NAC-8	938.47	616.86	65.73	34.27	3.3

4 mol L⁻¹ and 6 mol L⁻¹, respectively, the N₂ saturated adsorption capacity of modified NAC-2, NAC-4 and NAC-6 increased with the increase of HNO₃ concentration. This phenomenon indicated that the increase of HNO₃ concentration had a favorable effect on the microporous structure and specific surface area of AC. However, when the concentration of HNO₃ was 8 mol L⁻¹, the N₂ saturated adsorption capacity of modified NAC-8 decreased, which was lower than that of NAC-6, indicating that the increase of HNO₃ concentration had adverse effects on the microporous structure and specific surface area of AC at this condition.

When $P/P_0 > 0.45$, hysteresis loops with inconsistent adsorption and desorption curves were observed in the isotherm, indicating that the sample had obvious mesopore structure. In addition, it could be seen that with the increase of HNO₃ concentration, the mesoporous distribution range of modified AC became wider. As shown in Figure 3B, the pore size distribution of AC samples before and after modification exhibited that the proportion of micropore and mesoporous of modified AC increased compared with unmodified AC. When the concentration of HNO₃ was 6 mol L⁻¹, part of the micropore of NAC-6 began to develop into mesoporous, and the proportion of mesoporous was further increased. When the concentration of HNO₃ reached to 8 mol L⁻¹, the proportion of mesopore of NAC-8 increased significantly, while the proportion of micropore decreased. The above conclusion also confirmed the reason for the decrease of N₂ saturation adsorption capacity of modified NAC-8 in Figure 3A.

The structural parameters of AC modified with different HNO₃ concentrations could be seen in Table 1. The specific surface area (S_{BET}) of the raw NAC-0 was 905.72 m² g⁻¹, and the S_{BET} of the NAC-x (x = 2,4,6) samples after HNO₃ modification significantly increased to 949.62 m² g⁻¹, 983.51 m² g⁻¹ and 1,140.40 m² g⁻¹, respectively. Correspondingly, the S_{mic} of the micropore area of NAC-x (x = 2,4,6) also increased. The P_{mic} of the modified samples changed from 70.29% to 75.73%, 73.66%, and 70.52%, respectively. Although the micropore ratio P_{mic} of sample NAC-6 was basically the same as that of sample NAC-0, the number of micropores of sample NAC-6 was still significantly higher than that of unmodified sample NAC-0, considering the specific surface area S_{BET} and micropore area S_{mic}. However, the S_{mic} of NAC-8 showed a downward trend compared with that of

NAC-6, decreasing to 938.47 m²/g. In addition, the P_{mic} of NAC-8 micropore ratio also decreased to 65.73%. This indicated that the number of micropores in the sample NAC-8 was greatly reduced. However, at this time, the proportion of mesopores of NAC-8 increased sharply, and the number of P_{mes} reached 34.27%, indicating that NAC-8 generated more and larger mesoporous structures. This was because with the increase of HNO₃ concentration, some micropore of AC was expanded by the oxidation and the collapse of carbon skeleton structure under the strong oxidation of HNO₃, forming transition pores and increasing the proportion of mesoporous. At the same time, with the increase of HNO₃ concentration, the average pore size D of the modified NAC-x (x = 2,4,6,8) samples increased from 2.8 nm to 3.3 nm. Due to the reaction of HNO₃ with carbon, many previously closed mesoporous pores were opened, and the pore size of AC was increased by HNO₃ modification. In the process of adsorption and removal of small molecular polar organic pollutants in the gas phase, micropore played a major role in adsorption, while mesoporous played the role of channels. Abundant mesoporous were conducive to mass transfer of pollutants in AC. The larger the specific surface area of the sample, the richer the number of micropores, and the better the adsorption capacity of the sample. Therefore, the variation law of structural parameters of the modified AC sample NAC-x in Table 1 also confirmed the isothermal adsorption trend of Figure 3A.

3.2 Surface chemical properties

3.2.1 FTIR spectrum analysis

The number, type and position distribution of functional groups were very important to the adsorption performance of AC. In general, functional groups mainly existed on the microporous surface of AC. The FTIR spectrums of AC before and after modification were shown in Figure 4. The characteristic peak of the sample at 3,423 cm⁻¹ belonged to the phenolic O-H bond of the amino functional group (Zhang et al., 2015). Compared with the raw NAC-0, the characteristic peak of NAC-x sample at 3,423 cm⁻¹ showed that the infrared luminosity decreased with the increase of the impregnation concentration of HNO₃. Obviously, this was due to the

FIGURE 4
FTIR spectra of the as-prepared AC samples.
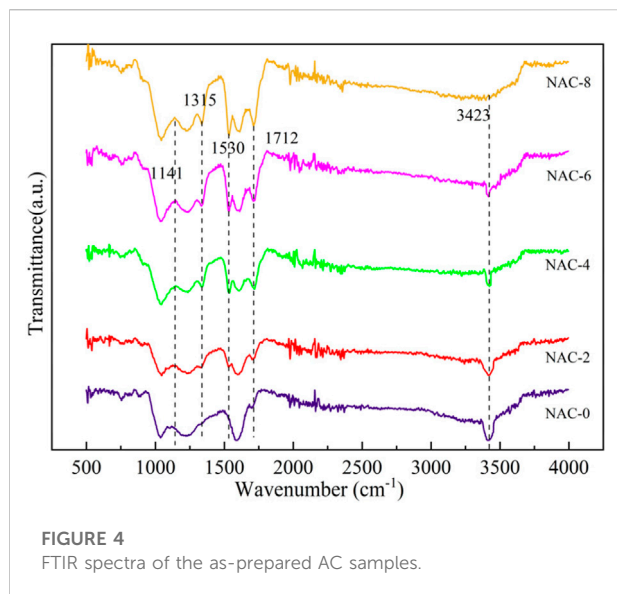
increased number of O-H bonds in the AC structure. Meanwhile, the absorption vibration peak of NAC-x sample at 1,712 cm^{-1} corresponded to the C=O stretching vibration peak of carboxyl group or carbonyl group, the absorption vibration peak at 1,530 cm^{-1} was the stretching vibration of C = O bond, and the characteristic peak at 1,315 cm^{-1} was the carbonyl group (Zhang et al., 2017; Cheng et al., 2018). The peak at 1,141 cm^{-1} belonged to C-O-C bond and -OH bond vibration of carboxylic anhydride (Nejabat and Rayati, 201s8).

In addition, the changes of these new vibration peaks were similar: with the increase of the impregnation concentration of HNO$_3$, the infrared luminosity of the corresponding modified NAC-x sample decreased, which indicated that the number of carboxy anhydride and the vibration of -OH bond increased. Therefore, it was inferred that CO and CO$_2$ were released after HNO$_3$ oxidation, which led to the AC ablation and the pore structure deformation. After O and H were adsorbed on the deformed pore structure, oxygen-containing functional groups, such as carboxyl groups and esters, were formed due to the increase of adsorption active sites (Li et al., 2015; Fang et al., 2017).

3.2.2 Boehm titration results of oxygen-containing functional groups

In order to quantify the content of functional groups on the surface of AC samples, Boehm titration analysis was performed. The specific changes of surface functional groups before and after modification were shown in Table 2. It could be seen that Boehm titration results were similar to the infrared spectrum analysis results. After HNO$_3$ oxidation modification, the contents of carboxyl and lactone groups on the sample surface enhanced significantly with the increase of HNO$_3$ concentration. The modified NAC-6

sample changed most dramatically with the carboxyl, lactone and hydroxyl increased by 0.230 mmol g^{-1}, 0.147 mmol g^{-1}, and 0.082 mmol g^{-1}, respectively. Meanwhile, the total acid oxygen-containing functional group content also increased from 0.208 mmol g^{-1} to 0.667 mmol g^{-1}, with an increase of 0.459 mmol g^{-1}, as shown in Figure 5. This indicated the content of acidic oxygen-containing groups on the surface of AC increased significantly after HNO$_3$ oxidation modification, which was more conducive to the absorption of gas-phase polar pollutants such as formaldehyde.

3.3 Adsorption capacity of AC samples

In the static adsorption experiment, the formaldehyde adsorption on AC before and after modification was measured by phenol reagent-spectrophotometry, and the test results were shown in Figure 6. The formaldehyde saturation adsorption capacity of unmodified NAC-0 was 546.73 μg g^{-1}. The saturated adsorption capacity of AC modified by HNO$_3$ varied with the concentration of HNO$_3$. When the concentration of HNO$_3$ was 6 mol L^{-1}, the saturation adsorption capacity of NAC-6 to formaldehyde reached the maximum of 963.67 μg g^{-1}.

However, when the concentration of HNO$_3$ reached to 8 mol L^{-1}, the saturated adsorption capacity of NAC-8 to formaldehyde decreased. This indicated that, after HNO$_3$ modification, the content of acidic oxygen-containing functional groups on the surface of AC samples increased, the number of mesoporous cells enlarged, and the channel function of mesoporous cells strengthened. But the proportion of micropores on AC decreased, which was not conducive to formaldehyde gas adsorption in terms of overall adsorption performance. In conclusion, the rapid modification of HNO$_3$ impregnation coupled with microwave radiation could promote the adsorption of formaldehyde gas on AC. The adsorption capacity of NAC-6 sample to formaldehyde was the strongest (963.67 μg g^{-1}), which was about 43% higher than that of raw NAC-0 (546.73 μg g^{-1}).

The real-time dynamic adsorption curve was drawn according to the formaldehyde adsorption amount of AC samples at different times, and the saturation time when the sample adsorption reached dynamic equilibrium was finally obtained. Figure 7 showed the dynamic adsorption curves of formaldehyde for AC samples before and after modification with different concentrations of HNO$_3$ under microwave radiation. At the initial stage of adsorption, the adsorption rate of formaldehyde on AC samples showed a rapid upward trend, and then the curve trend gradually tended to be flat with the growth of time. The slope of NAC-x curve was higher than that of the raw carbon NAC-0. This phenomenon indicated that HNO$_3$ coupled with microwave rapidly modified AC samples had a

TABLE 2 Quantitative characterization of the surface compositions of the as-prepared AC samples.

Samples	Carboxyl (mmol·g^{-1})	Lactone (mmol·g^{-1})	Hydroxyl (mmol·g^{-1})	Total acidic group (mmol·g^{-1})
NAC-0	0.077	0.089	0.042	0.208
NAC-2	0.245	0.200	0.059	0.504
NAC-4	0.283	0.191	0.100	0.574
NAC-6	0.307	0.236	0.124	0.667
NAC-8	0.242	0.190	0.203	0.635

FIGURE 5
Total acidic groups of the NAC-x samples.

FIGURE 7
Formaldehyde dynamic adsorption capacity of AC samples before and after modification.

FIGURE 6
Formaldehyde static adsorption capacity of AC samples before and after modification.
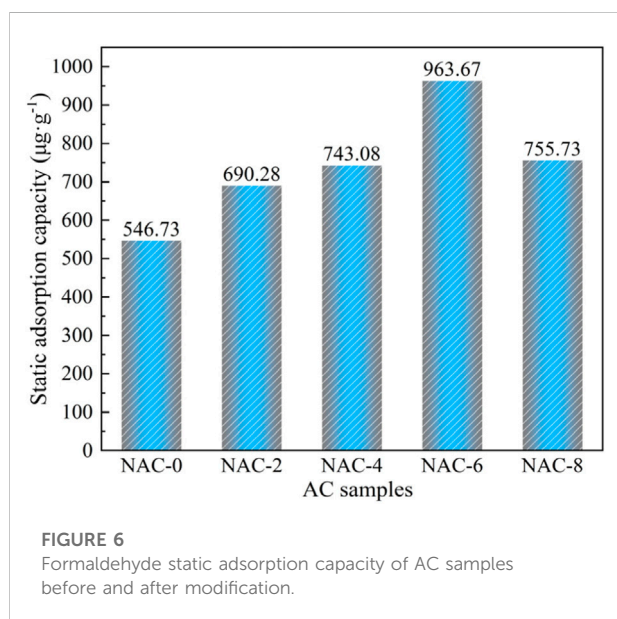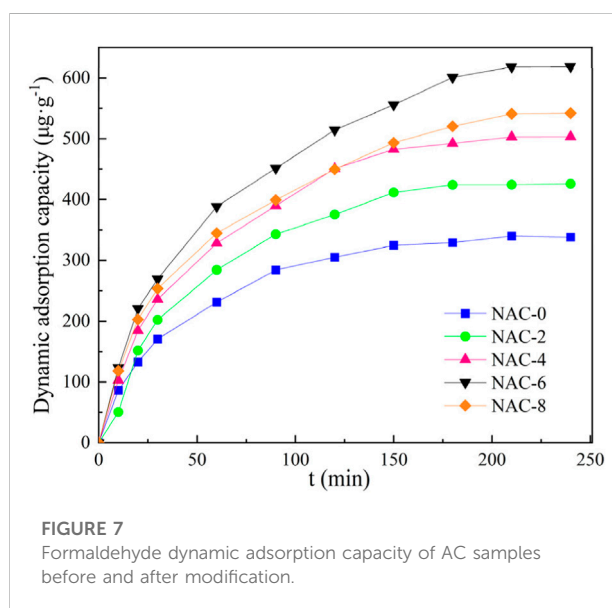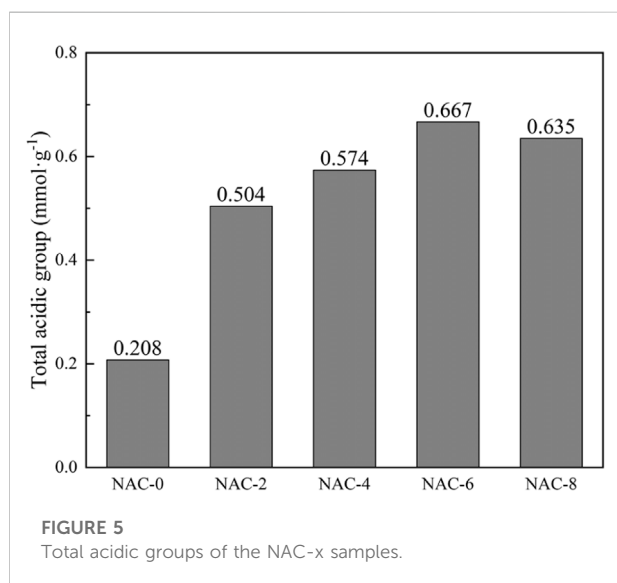
faster adsorption rate of formaldehyde. In addition, the trend of formaldehyde adsorption curve tended to be flat, which indicated that AC adsorption reached saturation at this moment. It could be seen that the formaldehyde saturated adsorption time of NAC-x was longer than that of NAC-0. The final formaldehyde saturation adsorption capacity of the modified AC sample NAC-6 was the largest among the five test samples. The adsorption of formaldehyde on the surface of AC depended on its diffusion in pores. Instantaneous adsorption or external surface adsorption was the result of superposition of adsorption fields, where diffusion was the strongest. During the slow adsorption stage, the internal diffusion of particles depended on the adsorption rate factor of this stage, the adsorption rate gradually slowed down at this period. The last stage was the final equilibrium stage, most of the pores were filled with adsorbents, the diffusion rate of internal particles further slowed down, the adsorption rate also further reduced and finally tended to be saturated.
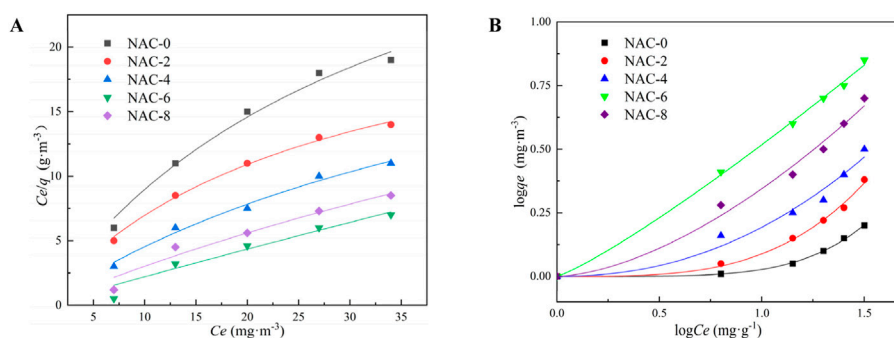
FIGURE 8
Adsorption isotherm model curve fitting AC adsorption experimental data: **(A)** Langmuir equation; **(B)** Freundlich equation.

TABLE 3 Fitting parameters of Langmuir equation and Freundlich equation.

Samples	Langmuir equation			Freundlich equation			
	$q_{max}/(\text{mg·g}^{-1})$	$\alpha/$ $(\text{m}^3\text{·mg}^{-1})$	R^2	k_f	n	R^2
NAC-0	0.47	0.24	0.992	0.17	2.53	0.999
NAC-2	0.32	0.16	0.988	0.16	3.22	0.995
NAC-4	0.22	0.11	0.998	0.28	2.07	0.975
NAC-6	0.26	0.13	0.976	0.42	2.09	0.989
NAC-8	0.34	0.21	0.959	0.31	1.27	0.958

3.4 Adsorption model fitting of AC samples

The c_e/q-c_e and $\log q_e$-$\log c_e$ fitting curves were drawn according to the adsorption models of the samples before and after modification, as shown in Figure 8, and the fitting parameters were summarized in Table 3. The fitting parameters of Langmuir equation and Freundlich equation could reflect the adsorption performance of formaldehyde to a certain extent. The adsorption model constant k_f of Freundlich isothermal adsorption equation reflected the adsorption capacity of AC samples. The larger k_f value, the stronger the adsorption capacity of the sample (Cheng and Bi, 2013). The adsorption model index n was always larger than 1, indicating preferential adsorption at this point. At this time, the key reason of the sample adsorption of formaldehyde was mainly chemical bond force rather than van der Waals force. It could be seen that HNO_3 coupling microwave rapid modification was conducive to the adsorption of formaldehyde on AC, and the adsorption performance of NAC-6 sample was the best.

The fitting results of the adsorption kinetic model were shown in Figure 9, and the relevant fitting parameters were

exhibited in Table 4. It can be seen from the fitting parameters that the fitting degree R^2 of the quasi-first-order adsorption kinetic model of modified AC samples under different HNO_3 concentrations coupled with microwave irradiation was relatively low. This demonstrated there was a deviation between the model fitting and the experimental data. The fitting degree R^2 of the quasi-second-order adsorption kinetic model of modified AC samples under different HNO_3 concentrations was larger than 0.99. This manifested the experimental data matched the quasi-second-order adsorption model better, which further reflected the formaldehyde adsorption of modified AC tended to be physical-chemical combined adsorption.

3.5 Mechanism analysis

Formaldehyde was a polar molecular substance with the carbonyl group of the polar functional group in formaldehyde, in which the π bond was very unstable and easily broken. Therefore, the existence of C=O group of formaldehyde made it easy to have addition reaction with oxygen-containing
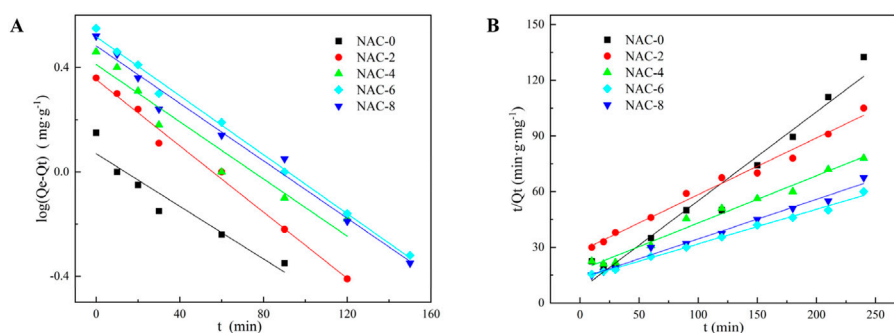
FIGURE 9
Adsorption kinetic model fitting AC adsorption experimental data: **(A)** Pesudo-first-order model; **(B)** Pesudo-second-order model.

TABLE 4 Fitting parameters of Pesudo first-order model and Pesudo second-order model.

Samples	Pseudo-first-order model			Pesudo second-order model		
	Q_e (mg·g^{-1})	k_1 (min^{-1})	R^2	Q_e (mg·g^{-1})	k_2 (g·mg^{-1}·min^{-1})	R^2
NAC-0	0.07	0.060	0.984	7.18	0.478	0.991
NAC-2	0.35	0.052	0.990	2.78	0.305	0.994
NAC-4	0.41	0.053	0.935	1.76	0.254	0.993
NAC-6	0.48	0.056	0.978	1.31	0.213	0.998
NAC-8	0.52	0.057	0.994	1.32	0.183	0.994
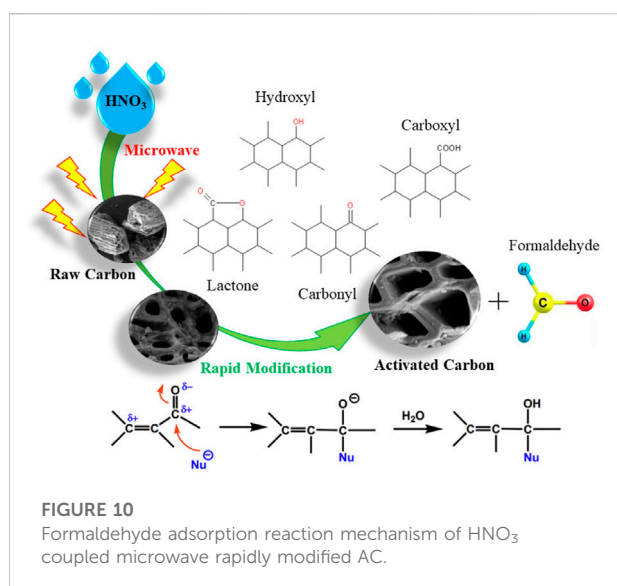
FIGURE 10
Formaldehyde adsorption reaction mechanism of HNO$_3$ coupled microwave rapidly modified AC.

functional groups. The type and quantity of oxygen-containing groups on the surface of AC which was a weakly polar substance, directly determined the polarity of

AC surface. The more acidic functional groups (such as carboxyl, lactone, hydroxyl and other acidic oxygen-containing groups), the stronger the AC polarity, and the more superior the adsorption capacity of AC for polar pollutants. After the modification of AC by HNO$_3$, more acidic oxygen-containing functional groups were introduced, and the number of carboxyl groups and lactone groups on the surface increased significantly, as well as the content of total acidic oxygen-containing groups, as shown in Figure 10. After the AC modification by HNO$_3$ coupled microwave, the number of carboxyl groups and lactone groups on the surface increased significantly, and the content of total acidic oxygen-containing groups also improved. Compared with NAC-0, the surface oxygen-containing functional groups of NAC-6 sample with HNO$_3$ concentration at 6 mol L^{-1} increased by 0.459 mmol g^{-1}. The main function of low concentration HNO$_3$ was to remove impurities in the AC pores, so that the pore structure of AC became clearer and more abundant. In addition, during the modification process, the low concentration of HNO$_3$ reacted with a small amount of basic oxygen-containing groups on the AC surface, which reduced the surface proportion of basic oxygen-containing groups of AC, and then increased the

proportion of acid oxygen-containing groups. In the modification process, with the increase of HNO_3 concentration, the content of acidic oxygen-containing functional groups on the AC surface increased, which enhanced the polarity of the sample surface and improved the adsorption performance of the sample to polar molecules. With the continuous increase of HNO_3 concentration, the oxidation of HNO_3 gradually occupied a dominant position. The oxidation and corrosion effects of HNO_3 on the pore structure of AC was progressively obvious, which adversely affected the specific surface area and micropore structure of AC. The above results were consistent with the adsorption isotherms and adsorption kinetics fitting results.

4 Conclusion

According to the above research results, it can be recognized that AC is able to be rapidly modified by HNO_3 immersion coupled with microwave irradiation. HNO_3 coupled with microwave can simultaneously regulate the surface functional groups and the internal pore structure of AC. The modified AC has abundant surface chemical groups and developed specific surface area, which greatly improves the adsorption capacity of biochar to polar substances.

In this experiment, the excellent adsorption performance of the modified samples was related to the different effects of HNO_3. On the one hand, the corrosion effect of HNO_3 is beneficial to obtain higher specific surface area and form more micropores on the basis of retaining the physical structure of the raw carbon. On the other hand, after adding HNO_3, the oxygen-containing functional groups on the surface of AC increased sharply, which enhanced the surface acidity and polarity of biochar, increased the adsorption active sites of AC and enhanced the adsorption activity. These factors also promote the adsorption and internal diffusion of formaldehyde molecules on AC surface, simultaneously. The specific surface area S_{BET} of NAC-6 sample reached 1,140.40 $m^2\,g^{-1}$, and the increment of the total acid oxygen-containing functional groups was 0.459 mmol g^{-1} compared with the unmodified raw carbon. Meanwhile, NAC-6 sample had the best adsorption performance for formaldehyde, and the saturated adsorption capacity was 963.67 μg g^{-1}, which was 43% higher than that of the raw carbon. The adsorption behavior of formaldehyde on modified AC fitted well with the Langmuir model and the Freundlich model, in line with the basic requirements of adsorption mechanism. In addition, the kinetic data of formaldehyde adsorption of the modified AC samples matched the quasi-second-order fitting model, and the fitting degree was very high, which satisfied the law of physical-chemical combined adsorption.

Data availability statement

The original contributions presented in the study are included in the article/Supplementary Material, further inquiries can be directed to the corresponding author.

Author contributions

Conceptualization, YG, ZZ, and BC; methodology, XR and QC; validation, XD; formal analysis, XR and QC; investigation, MY, SL, and QW; resources, YG.; data curation, XD; writing—original draft preparation, XR and QC; writing—review and editing, YG, XD, and HD.; supervision, YG, ZZ, and BC; project administration, YG; funding acquisition, YG and BC. All authors have read and agreed to the published version of the manuscript.

Funding

Conflict of interest

XR was employed by Shandong High Speed Maintenance Group Co. Ltd. XD was employed by Shandong Luqiao Group Equipment Technology Development Company.

The remaining authors declare that the research was conducted in the absence of any commercial or financial relationships that could be construed as a potential conflict of interest.

Publisher's note

References

Abdulrasheed, A. A., Jalil, A. A., Triwahyono, S., Zaini, M. A. A., Gambo, Y., and Ibrahim, M. (2018). Surface modification of activated carbon for adsorption of SO2 and nox: A review of existing and emerging technologies. *Renew. Sustain. Energy Rev.* 94, 1067–1085. doi:10.1016/j.rser.2018.07.011

Alslaibi, T. M., Abustan, I., Ahmad, M. A., and Foul, A. A. (2014). Comparison of activated carbon prepared from olive stones by microwave and conventional heating for iron (II), lead (II), and copper (II) removal from synthetic wastewater. *Environ. Prog. Sustain. Energy* 33 (4), 1074–1085. doi:10.1002/ep.11877

Awadallah, F. A., and Al-Muhtaseb, S. A. (2019). Effect of gas templating of resorcinol-formaldehyde xerogels on characteristics and performances of subsequent activated carbons. *Mater. Chem. Phys.* 234, 361–368. doi:10.1016/j.matchemphys.2019.03.010

Cai, Y. J., Luo, Y., Xiao, Y., Zhao, X., Liang, Y., Hu, H., et al. (2016). Facile synthesis of three-dimensional heteroatom-doped and hierarchical egg-box-like carbons derived from moringa oleifera branches for high-performance supercapacitors. *ACS Appl. Mat. Interfaces* 8 (48), 33060–33071. doi:10.1021/acsami.6b10893

Chang, S. M., Hu, S. C., Shiue, A., Lee, P. Y., and Leggett, G. (2020). Adsorption of silver nano-particles modified activated carbon filter media for indoor formaldehyde removal. *Chem. Phys. Lett.* 757, 137864. doi:10.1016/j.cplett.2020.137864

Cheng, X., and Bi, X. T. (2013). Modeling and simulation of nitrogen oxides adsorption in fluidized bed reactors. *Chem. Eng. Sci.* 96, 42–54. doi:10.1016/j.ces.2013.03.052

Cheng, X., Cheng, Y., Wang, Z., and Ma, C. (2018). Comparative study of coal based catalysts for NO adsorption and NO reduction by CO. *Fuel* 214, 230–241. doi:10.1016/j.fuel.2017.11.009

Civioc, R., Lattuada, M., Koebel, M. M., and Galmarini, S. (2020). Monolithic resorcinol-formaldehyde alcogels and their corresponding nitrogen-doped activated carbons. *J. Solgel. Sci. Technol.* 95 (3), 719–732. doi:10.1007/s10971-020-05288-x

Demiral, I, Samdan, C., and Demiral, H. (2021). Enrichment of the surface functional groups of activated carbon by modification method. *Surfaces Interfaces* 22, 14 100873. doi:10.1016/j.surfin.2020.100873

Du, X., Li, C., Zhao, L., Zhang, J., Gao, L., Sheng, J., et al. (2018). Promotional removal of HCHO from simulated flue gas over Mn-Fe oxides modified activated coke. *Appl. Catal. B Environ.* 232, 37–48. doi:10.1016/j.apcatb.2018.03.034

Fang, R., Huang, H., Huang, W., Ji, J., Feng, Q., Shu, Y., et al. (2017). Influence of peracetic acid modification on the physicochemical properties of activated carbon and its performance in the ozone-catalytic oxidation of gaseous benzene. *Appl. Surf. Sci.* 420, 905–910. doi:10.1016/j.apsusc.2017.05.228

Gao, Y., Cao, Q., Guan, N., Zhang, Z., Fan, G., Dou, H., et al. (2022). Metal-organic framework supporting Fe3O4 prepared by microwave in couple with NTP to eliminate VOCs from biofuel. *Front. Energy Res.* 10. doi:10.3389/fenrg.2022.936493

Gao, Y., Luan, T., Zhang, M., Zhang, W., and Feng, W. (2018). Structure–activity relationship study of Mn/Fe ratio effects on Mn–Fe–Ce–Ox/γ-Al2O3 nanocatalyst for NO oxidation and fast SCR reaction. *Catalysts* 8 (12), 642. doi:10.3390/catal8120642

Gao, Y., Luan, T., Zhang, S., Jiang, W., Feng, W., and Jiang, H. (2019). Comprehensive comparison between nanocatalysts of Mn-Co/TiO2 and Mn-Fe/TiO2 for NO catalytic conversion: An insight from nanostructure, performance, kinetics, and thermodynamics. *Catalysts* 9 (2), 175. doi:10.3390/catal9020175

Gao, Y., Peng, X., Zhang, Z., Zhang, W., Li, H., Chen, B., et al. (2021). Ternary mixed-oxide synergy effects of nano TiO2-FexOy-MOk (M = Mn, Ce, Co) on alpha-pinene catalytic oxidation process assisted by nonthermal plasma. *Mat. Res. Express* 8 (1), 015509. doi:10.1088/2053-1591/abdbf7

Giraldo, L., Vargas, D. P., Moreno-Pirajan, J. C., Mancin, F., and Madder, A. (2020). Exploiting double exchange diels-alder cycloadditions for immobilization of peptide nucleic acids on gold nanoparticles. *Front. Chem.* 8, 4. doi:10.3389/fchem.2020.00004

Hu, M., Wu, W., Lin, D., and Yang, K. (2022). Adsorption of fulvic acid on mesopore-rich activated carbon with high surface area. *Sci. Total Environ.* 838, 155918. doi:10.1016/j.scitotenv.2022.155918

Inal, I. I. G., Gokce, Y., Yagmur, E., and Aktas, Z. (2020). Investigation of supercapacitor performance of the biomass based activated carbon modified with nitric acid. *J. Fac. Eng. Archit. Gazi Univ.* 35 (3), 1243–1255. doi:10.17341/gazimmfd.425990

Isinkaralar, K., Gullu, G., and Turkyilmaz, A. (2022). Experimental study of formaldehyde and BTEX adsorption onto activated carbon from lignocellulosic biomass. *Biomass Convers. biorefin.* 11. doi:10.1007/s13399-021-02287-y

Khasri, A., and Ahmad, M. A. (2018). Adsorption of basic and reactive dyes from aqueous solution onto intsia bijuga sawdust-based activated carbon: Batch and column study. *Environ. Sci. Pollut. Res.* 25 (31), 31508–31519. doi:10.1007/s11356-018-3046-3

Li, B. Z., Yang, Y. C., Wu, H. Y., Zhang, C., Zheng, W., and Sun, D. K. (2020). Adsorptive removal and mechanism of monocyclic aromatics by activated carbons from water: Effects of structure and surface chemistry. *Colloids Surfaces A Physicochem. Eng. Aspects* 605, 10 125346. doi:10.1016/j.colsurfa.2020.125346

Li, C.-j., Zhao, R., Peng, M.-q., Hao, L. I. U., Gang, Y. U., and Dong-sheng, X. I. A. (2015). Study on desulfurization and denitrification by modified activated carbon fibers with visible-light photocatalysis. *J. Fuel Chem. Technol.* 43 (12), 1516–1522. doi:10.1016/s1872-5813(16)30004-4

Li, L., Tang, L., Liang, X., Liu, Z., and Yang, Y. (2016). Adsorption performance of acetone on activated carbon modified by microwave heating and alkali treatment. *J. Chem. Eng. Jpn./. JCEJ.* 49 (11), 958–966. doi:10.1252/jcej.15we333

Liang, W. Y., Dong, J. F., Yao, M. Q., Fu, J. S., Chen, H. L., and Zhang, X. M. (2020). Enhancing the selectivity of Pd/C catalysts for the direct synthesis of H2O2 by HNO3 pretreatment. *New J. Chem.* 44 (43), 18579–18587. doi:10.1039/d0nj03820b

Nejabat, F., and Rayati, S. (2018). Surface modification of multi-walled carbon nanotubes to produce a new bimetallic Fe/Mn catalyst for the aerobic oxidation of hydrocarbons. *J. Industrial Eng. Chem.* 69, 324–330. doi:10.1016/j.jiec.2018.09.044

Prokic, D., Vukcevic, M., Kalijadis, A., Maletic, M., Babic, B., and Durkic, T. (2020). Removal of estrone, 17 beta-estradiol, and 17 alpha-ethinylestradiol from water by adsorption onto chemically modified activated carbon cloths. *Fibers Polym.* 21 (10), 2263–2274. doi:10.1007/s12221-020-9758-2

Qu, Y., Xu, L., Chen, Y., Sun, S., Wang, Y., and Guo, L. (2021). Efficient toluene adsorption/desorption on biochar derived from *in situ* acid-treated sugarcane bagasse. *Environ. Sci. Pollut. Res.* 28 (44), 62616–62627. doi:10.1007/s11356-021-15128-2

Rungrodnimitchai, S., and Hiranphinyophat, S. (2020). The functionalization of activated carbon by oxidation. *Key Eng. Mat.* 846, 251–256. doi:10.4028/www.scientific.net/kem.846.251

Ryu, D. Y., Kim, D. W., Kang, Y. J., Lee, Y., Nakabayashi, K., Miyawaki, J., et al. (2022). Preparation of environmental-friendly N-rich chitin-derived activated carbon for the removal of formaldehyde. *Carbon Lett.* 32, 1473–1479. doi:10.1007/s42823-022-00379-x

Saqlain, S., Zhao, S. F., Kim, S. Y., and Kim, Y. D. (2021). Enhanced removal efficiency of toluene over activated carbon under visible light. *J. Hazard. Mater.* 418, 11 126317. doi:10.1016/j.jhazmat.2021.126317

Shao, W., Zhang, H., Wan, D., Zhang, X. X., and Chang, N. (2019). Preparation of MnO2@P(AN-VDC)/AC composite fibers for high capacity formaldehyde removal. *Mater. Lett.* 242, 51–54. doi:10.1016/j.matlet.2019.01.092

Tan, C., Zuo, S. L., Zhao, Y. Y., and Shen, B. S. (2019). Preparation of multicolored carbon quantum dots using HNO3/HClO4 oxidation of graphitized carbon. *J. Mat. Res.* 34 (20), 3428–3438. doi:10.1557/jmr.2019.261

Toledo, R. B., Aragon-Tobar, C. F., Gamez, S., and de la Torre, E. (2020). Reactivation process of activated carbons: Effect on the mechanical and adsorptive properties. *Molecules* 25 (7), 18 1681. doi:10.3390/molecules25071681

Vikrant, K., Na, C.-J., Younis, S. A., Kim, K.-H., and Kumar, S. (2019a). Evidence for superiority of conventional adsorbents in the sorptive removal of gaseous benzene under real-world conditions: Test of activated carbon against novel metal-organic frameworks. *J. Clean. Prod.* 235, 1090–1102. doi:10.1016/j.jclepro.2019.07.038

Vikrant, K., Park, C. M., Kim, K.-H., Kumar, S., and Jeon, E.-C. (2019b). Recent advancements in photocatalyst-based platforms for the destruction of gaseous benzene: Performance evaluation of different modes of photocatalytic operations and against adsorption techniques. *J. Photochem. Photobiol. C Photochem. Rev.* 41, 100316. doi:10.1016/j.jphotochemrev.2019.08.003

Yang, Z. G., Yan, G. J., Liu, X. P., Feng, Z. Y., Zhu, X. F., Mao, Y. L., et al. (2022). Study on coconut shell activated carbon temperature swing adsorption of benzene and formaldehyde. *J. Renew. Mat.* 10 (12), 3573–3585. doi:10.32604/jrm.2022.022031

Yu, Z., Wang, D., Yang, Y., Meng, X., Liu, N. W., and Shi, L. (2019). Excellent adsorption performance of dibenzothiophene on functionalized low-cost activated carbons with different oxidation methods. *Environ. Technol.* 40 (13), 1686–1696. doi:10.1080/09593330.2018.1427802

Zahed, M., Jafari, D., and Esfandyari, M. (2022). Adsorption of formaldehyde from aqueous solution using activated carbon prepared from Hibiscus rosa-sinensis. *Int. J. Environ. Anal. Chem.* 102 (13), 2979–3001. doi:10.1080/03067319.2020.1762872

Zhang, D. D., Zhang, M. X., Ding, F., Liu, W., Zhang, L., and Cui, L. Z. (2020). Efficient removal of formaldehyde by polyethyleneimine modified activated carbon in a fixed bed. *Environ. Sci. Pollut. Res.* 27 (15), 18109–18116. doi:10.1007/s11356-020-08019-5

Zhang, L., Cui, L., Wang, Z., and Dong, Y. (2016). Modification of activated carbon using microwave radiation and its effects on the adsorption of SO<sub>2</sub>. *J. Chem. Eng. Jpn./. JCEJ.* 49 (1), 52–59. doi:10.1252/jcej.14we081

Zhang, M., Gao, Y., Mao, Y., Wang, W., Sun, J., Song, Z., et al. (2023). Enhanced dry reforming of methane by microwave-mediated confined catalysis over Ni-La/AC catalyst. *Chem. Eng. J.* 451, 138616. doi:10.1016/j.cej.2022.138616

Zhang, X., Gao, B., Creamer, A. E., Cao, C., and Li, Y. (2017). Adsorption of VOCs onto engineered carbon materials: A review. *J. Hazard. Mater.* 338, 102–123. doi:10.1016/j.jhazmat.2017.05.013

Zhang, X., Lv, X., Shi, X., Yang, Y., and Yang, Y. (2019). Enhanced hydrophobic UiO-66 (University of Oslo 66) metal-organic framework with high capacity and selectivity for toluene capture from high humid air. *J. Colloid Interface Sci.* 539, 152–160. doi:10.1016/j.jcis.2018.12.056

Zhang, X., Zhang, S., Yang, H., Shao, J., Chen, Y., Feng, Y., et al. (2015). Effects of hydrofluoric acid pre-deashing of rice husk on physicochemical properties and CO2 adsorption performance of nitrogen-enriched biochar. *Energy* 91, 903–910. doi:10.1016/j.energy.2015.08.028

Zhu, J. W., Chen, J., Zhuang, P. Y., Zhang, Y. Y., Wang, Y. B., Tan, H. Z., et al. (2021). Efficient adsorption of trace formaldehyde by polyaniline/TiO2 composite at room temperature and mechanism investigation. *Atmos. Pollut. Res.* 12 (2), 1–11. doi:10.1016/j.apr.2020.09.015